POLITECNICO DI TORINO
Repository ISTITUZIONALE

Development of new analytical tools for tritium transport modelling

Original
Development of new analytical tools for tritium transport modelling / Alberghi, C., Candido, L., Utili, M., Zucchetti, M.. - In: FUSION ENGINEERING AND DESIGN. - ISSN 0920-3796. - ELETTRONICO. - 177:(2022), p. 113083. [10.1016/j.fusengdes.2022.113083]

Availability:
This version is available at: 11583/2957914 since: 2022-05-11T08:33:07Z

Publisher:
Elsevier

Published
DOI:10.1016/j.fusengdes.2022.113083

Terms of use:

This article is made available under terms and conditions as specified in the corresponding bibliographic description in the repository

Publisher copyright
Elsevier postprint/Author's Accepted Manuscript

© 2022. This manuscript version is made available under the CC-BY-NC-ND 4.0 license http://creativecommons.org/licenses/by-nc-nd/4.0/.The final authenticated version is available online at: http://dx.doi.org/10.1016/j.fusengdes.2022.113083

(Article begins on next page)

06 October 2026

Development of new analytical tools for tritium transport modelling

Ciro Alberghi[a,*], Luigi Candido[a], M. Utili[b], M. Zucchetti[a,c]

[a] *ESSENTIAL Group, Politecnico di Torino - Corso Duca degli Abruzzi, 24, 10129, Torino, Italy*
[b] *ENEA C.R. Brasimone – Località Brasimone, 40043 Camugnano (BO), Italy*
[c] *Plasma Science and Fusion Center, Massachusetts Institute of Technology - 167 Albany St, 02139 Cambridge (MA), US*

Abstract

Tritium technologies, in particular tritium extraction from lithium-lead (LiPb, 15.7 at. % Li) and tritium concentration measurement in the eutectic alloy, are among the most challenging aspects of the R&D activities envisaged for the development of ITER and the European DEMO reactor. For instance, to efficiently design the systems devoted to the extraction of tritium, such as Gas-Liquid Contactors (GLC), Permeators Against Vacuum (PAV) or Liquid-Vacuum Contactor (LVC), theoretical models for the evaluation of the permeation flux are strictly necessary. In general, the same needs arise for the description of tritium permeators, which can find their application as Hydrogen isotopes Permeation Sensors (HPS) for the measurement hydrogen/tritium solubilized in the LiPb of either the Test Blanket Systems (TBS) or the Breeding Blanket. In this paper, new mathematical tools to describe the different permeation regimes both in the gas phase and in the presence of hydrogen isotopes monoatomically dissolved in a liquid phase, thus substantiating the theoretical background of hydrogen isotopes transport modelling throughout a membrane, is presented. For the sake of completeness, theoretical models in case of absence of a membrane (LVC) are also reported.

Keywords: Hydrogen Isotopes, Permeation, Membranes, PAV, LVC, Tritium modeling

1. Introduction

Over the last two decades, there has been a surge of interest in developing technologies for measuring and extracting tritium from liquid LiPb. For example, ENEA C. R. Brasimone, in collaboration with Politecnico di Torino, has developed hydrogen isotopes Permeation Sensors (HPS) based on pure α-iron membranes since the 2000s [1, 2, 3]; these sensors have been characterised under both static and flowing LiPb conditions [4]. As for the tritium extraction technologies, several technologies have been studied and developed [5, 6], such as the Gas-Liquid Contactor (GLC), the Permeator Against Vacuum (PAV) and the Liquid-Vacuum Contactor (LVC) [7, 8, 9]. Among these, the PAV concept should be highlighted as it is one of the reference technologies envisaged for the European reactor DEMO [10].

As far as modelling is concerned, most analytical models have been developed for gas-driven permeation [11, 12, 13]. The permeation of hydrogen through a membrane is called gas-driven permeation because the permeation is induced by the pressure gradient of the hydrogen gas between the upstream (or high pressure) side and the downstream (or low pressure) side. In general, the permeation of hydrogen isotopes is influenced by at least four factors: diffusivity, solubility, surface adsorption and desorption, and hydrogen-defects interaction. Neglecting the presence of structure defects or trapping sites, one can identify two limiting regimes: the diffusion-limited regime (DLR) and the surface-limited regime (SLR) [14]. Additional references can be found in [15, 16, 17]. For the so-called Plasma-Facing Components (PFC), trapping was implemented in 1D and 2D numerical codes [18, 19, 20, 21, 22, 23, 24]. However, if the upstream side is LiPb (or more generally a liquid metal or molten salt), the hydrogen isotopes are monoatomically dissolved into the liquid. To account for transport in the liquid phase, a mass transfer coefficient is usually assumed in this framework. Recently, Humrickhouse and Merril [25] have developed an analytical model that takes into account the mass transfer coefficient of tritium in LiPb assuming a DLR. However, this assumption does not always hold - especially for permeators based on V-group metals - as surface effects can play a major role. To solve this problem and to substantiate the theoretical physical background of tritium transport, new analytical models are presented within the paper.

2. Hydrogen isotopes transport in permeators

2.1. Gas-solid-gas systems

In gas-solid-gas permeators, hydrogen isotope atoms are in diatomic form at the high pressure side. A metal membrane separates this from one side, which is generally kept under vacuum. Thanks to the pressure gradient, a

*Corresponding author
Email address: ciro.alberghi@polito.it (Ciro Alberghi)

flux is promoted between the two sides. In Fig. 1 the phenomena described are shown schematically. It should be highlighted that this model assumes equal recombination constants at both sides of the membrane.

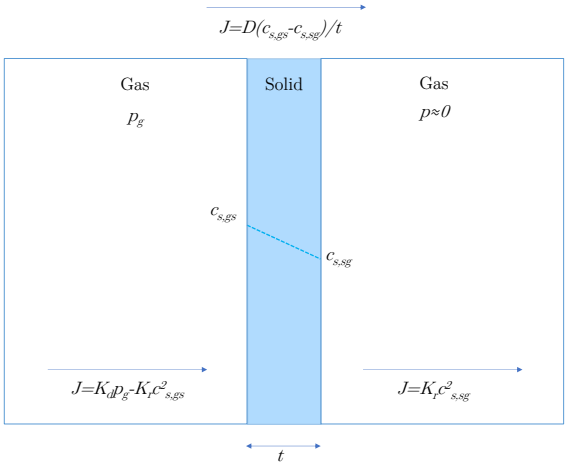

Figure 1: Typical concentration behavior in a gas-solid-gas permeator. The molar fluxes in the three different domains are shown.

The molar flux impinging on the left side of the membrane is determined by the following equation, which reads:

$$J = K_d p_g - K_r c_{s,gs}^2 \tag{1}$$

where p_g (Pa) is the tritium partial pressure in the gas, $c_{s,gs}$ (mol m^{-3}) is tritium concentration in the membrane on the gas-solid interface. K_d (mol m^{-2} s^{-1} Pa^{-1}) and K_r (m^4 mol^{-1} s^{-1}) are the dissociation and recombination constants, respectively. The flux across the membrane is given by:

$$J = \frac{D}{t}\left(c_{s,gs} - c_{s,sg}\right) \tag{2}$$

Here, D (m^2 s^{-1}) is the diffusion coefficient, t (m) is the thickness of the membrane, $c_{s,sg}$ (mol m^{-3}) is the concentration on the right side of the membrane. On the vacuum side, in the case in which $p \approx 0$, the flux is:

$$J = K_r c_{s,sg}^2 \tag{3}$$

The fluxes are now non-dimensionalised (denoted by the apex *) by dividing their values by $DK_{s,s}\sqrt{p_g}/t$, where $K_{s,s}$ (mol m^{-3} Pa$^{-1/2}$) is the Sieverts' constant of the membrane, while the concentrations are non-dimensionalised by the factor $K_{s,s}\sqrt{p}$. This results in:

$$J^* = W\left(1 - c_{s,gs}^{*2}\right) \tag{4}$$

$$J^* = c_{s,gs}^* - c_{s,sg}^* \tag{5}$$

$$J^* = W c_{s,sg}^{*2} \tag{6}$$

The dimensionless number $W = K_r K_s t p_g^{1/2}/D$ is called *permeation parameter* [14]. In steady-state, the three fluxes must be equal. The solution of the problem is given by the following system of equations:

$$c_{s,gs}^* = \sqrt{1 - c_{s,sg}^{*2}} \tag{7}$$

$$W^2 c_{s,sg}^{*4} + 2W c_{s,sg}^{*3} + 2c_{s,sg}^{*2} = 1 \tag{8}$$

Simple solutions can be found in two limiting cases. For small values of W, the flux is limited by surface effects, and it results:

$$J^* = \frac{1}{2}W \tag{9}$$

or $J = 1/2 K_d p_g$ in dimensional form. The dissociation constant, the recombination constant and the Sieverts' constant are related, in equilibrium conditions (but is assumed to be valid also outside equilibrium), through the relationship $K_{s,s} = (K_d/K_r)^{0.5}$. The permeation regime is called surface-limited regime (SLR) and $c_{s,gs} = c_{s,sg} = K_{s,s}\sqrt{p_g/2}$. Otherwise, for $W \gg 1$ the diffusion in the bulk of the membrane is rate-limiting. The dimensionless flux becomes:

$$J^* = 1 \tag{10}$$

that in dimensional form is $J = DK_{s,s}\sqrt{p_g}/t$. The permeation regime is called diffusion-limited regime (DLR) and the concentrations takes the values $c_{s,gs} = K_{s,s}\sqrt{p_g}$ and $c_{s,sg} = 0$.

In Fig. 6, the relative error of the limit solutions with respect to the full solution, obtained substituting the meaningfull roots of Eq. 8 in Equation 6, is plotted as a function of W.

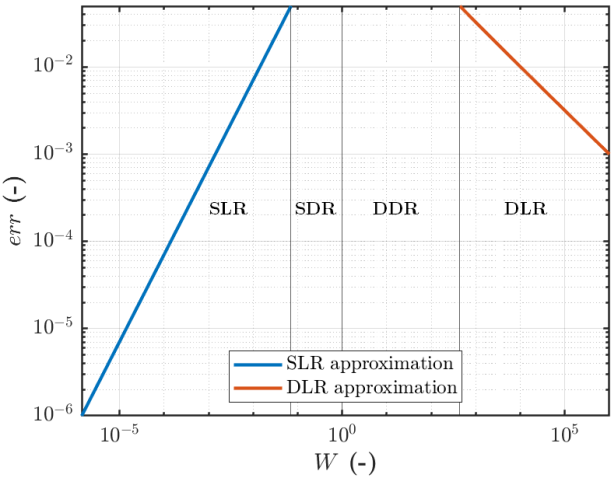

Figure 2: Relative error (-) between the limit regimes solution and the full solution, cut at $err = 0.05$.

The figure is cut at $err > 0.05$, which is considered here to be the maximum acceptable error that allows the limiting

case formulae for dimensionless flux to be adopted. Four regions are then defined: for $W < 7 \cdot 10^{-2}$ the surface-limited regime takes place, whereas for $W > 4 \cdot 10^{2}$ the kinetics is diffusion-limited. Around $W = 1$, two mixed regime, named surface-dominating regime (SDR) and diffusion-dominating regime (DDR) can be defined, extending the analysis proposed by Candido *et. al.*. [4]. It is interesting to highlight that surface effects are negligible only for permeation parameters in the order of hundreds.

2.2. Liquid-gas system

In liquid-vacuum contactors (LVC), hydrogen isotope atoms are monoatomically dissolved in a liquid that is in contact with the gas-phase, kept under vacuum, where the extracted hydrogen flows due to the pressure gradient. In Figure 3 the hydrogen concentration and flux, in the different domains, are depicted.

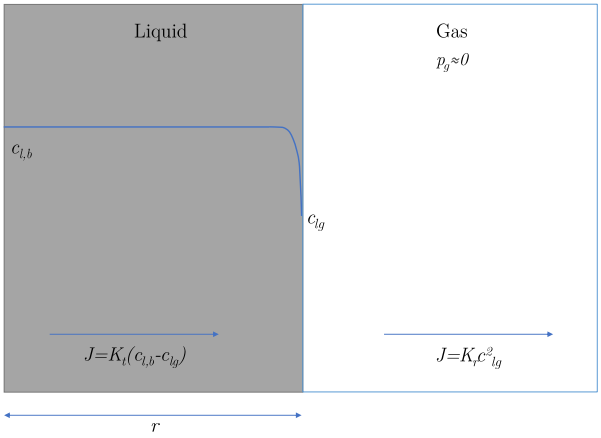

Figure 3: Typical concentration behavior in a liquid-gas permeator. The molar fluxes in the two different domains are shown.

The relationship for steady-state flux through a liquid-gas system for 1D slab is now derived. The flux moving in the liquid is determined by:

$$J = K_t \left(c_{l,b} - c_{lg}\right) \tag{11}$$

which is the analogous of Eq. 21, with $c_{l,b}$ and c_{lg} bulk concentration and liquid-gas interface concentration, respectively. The flux departing from the liquid surface is defined as:

$$J = K_r c_{lg}^2 \tag{12}$$

Here K_r is the recombination constant referred to the liquid surface. The fluxes are now non-dimensionalised by dividing their value by $K_t c_{l,b}$, and the concentrations by: $c_{l,b} = K_{s,l}\sqrt{p_l}$:

$$J^* = 1 - c_{lg}^* \tag{13}$$

$$J^* = \frac{1}{C} c_{lg}^{*2} \tag{14}$$

C is called by us *contact parameter*, and is defined as:

$$C = \frac{K_t}{K_r} \frac{1}{K_{s,l}\sqrt{p_l}} \tag{15}$$

At steady-state, the fluxes Eqs. 13 and 14 must be equal, giving the following second-degree algebraic equation:

$$\frac{1}{C} c_{lg}^{*2} + c_{lg}^* - 1 = 0 \tag{16}$$

that determines the dimensionless interface concentration c_{lg}^*:

$$c_{lg}^* = \frac{\pm\sqrt{1 + 4/C} - 1}{2/C} \tag{17}$$

The negative solution is unphysical, therefore it is neglected. The non-dimensional flux for a liquid-gas system can be derived injecting the latter equation in Eq. 14:

$$J^* = \frac{\left(\sqrt{1 + 4/C} - 1\right)^2}{4/C} \tag{18}$$

It is interesting to see that the relation of the flux is equivalent to Eq. 33, when W is exchanged with $1/C$.

There are two limiting cases: when $C \ll 1$, the mass transfer in the liquid is the slowest phenomenon, and the transport regime is liquid-limited (LLR). In this case the flux becomes:

$$J^* = 1 \tag{19}$$

which in dimensional form is $J = K_t c_{l,b}$, and $c_{lg} \approx 0$. In the other case, $C \gg 1$, surface effects dominate the kinetics, so the regime is surface-limited (SLR). The flux becomes:

$$J^* = \frac{1}{C} \tag{20}$$

This means that the interface concentration is $c_{lg} = c_{l,b}$ and the dimensional flux is $J = K_r c_{l,b}^2 = K_r K_{s,l}^2 p_l$.

In Fig. 4, the relative error of the limit solutions with respect to the full solution, Eq. 18, is plotted as a function of C.
The figure is cut at $err > 0.05$, which is considered here to be the maximum acceptable error that allows the limiting case formulae for dimensionless flux to be adopted. Four regions are then defined: for $C < 2 \cdot 10^{-3}$ the liquid-limited regime takes place, whereas for $C > 4 \cdot 10^{1}$ the kinetics is surface-limited. Around $C = 1$, the liquid-dominating regime and diffusion-dominating regime can be found.

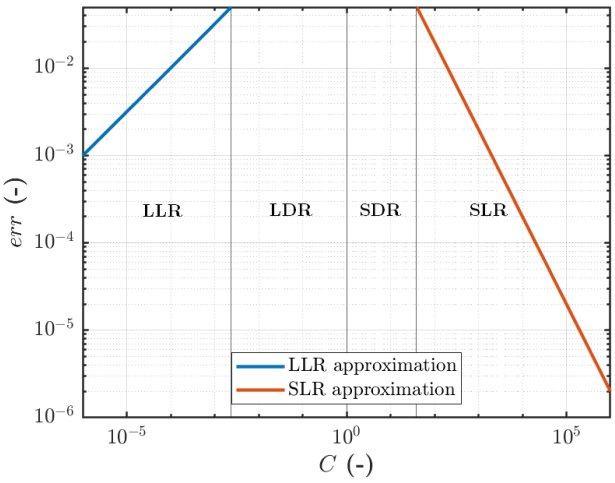

Figure 4: Relative error (-) between the limit regimes solution and the full solution, cut at $err = 0.05$.

2.3. Liquid-solid-gas systems

In the systems under consideration, hydrogen isotope atoms are monoatomically dissolved in a liquid, usually a molten metal or salt, from which they must be removed (PAV extractor technology) or measured (sensor technology). A metal membrane separates the stagnant or flowing liquid from a side where the pressure of the hydrogen isotope Q_2 is kept at lower values, generally under vacuum. Thanks to the pressure gradient, a flux is promoted between the two sides. In Fig. 5 the phenomena described are shown schematically.

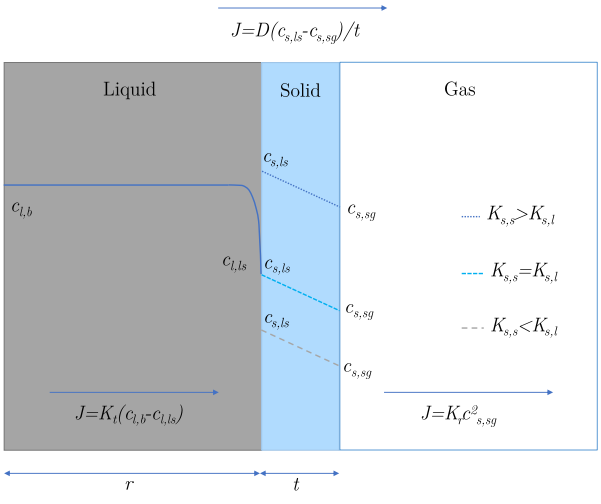

Figure 5: Typical concentration behavior in a liquid-solid-gas permeator. The molar fluxes in the three different domains are shown.

A relationship for steady-state flux through a liquid-solid-gas system for a simple 1D slab is now derived. The flux moving in the liquid can be determined, if the mass transfer coefficient K_t (m s^{-1}) is known, by:

$$J = K_t \left(c_{l,b} - c_{l,ls}\right) \tag{21}$$

where $c_{l,b}$ and $c_{l,ls}$ are the tritium concentrations in the bulk of the liquid and at the liquid-solid interface, respectively. The flux through the membrane is instead given by the expression:

$$J = \frac{D}{t}\left(c_{s,ls} - c_{s,sg}\right) \tag{22}$$

Here $c_{s,ls}$ and $c_{s,sg}$ are the concentrations in the membrane at the liquid-solid and solid-gas interfaces. The concentrations $c_{l,ls}$ and $c_{s,ls}$ are related by pressure continuity at the interface between the liquid and the membrane $p_{l,ls} = p_{s,ls}$, where $p_{l,ls}$ is the partial pressure of the hydrogen isotope, evaluated at the liquid/solid interface, and $p_{s,ls}$ is the partial pressure at the solid/liquid interface, from which, taking Sieverts' law $c = K_s\sqrt{p}$ into account, the concentration discontinuity at the interface results:

$$\frac{c_{l,ls}}{c_{s,ls}} = \frac{K_{s,l}}{K_{s,s}} \tag{23}$$

The ratio $K = K_{s,s}/K_{s,l}$ is called *partition coefficient*. The last flux is that departing from the membrane, which is the same in the case where the gas side is kept at a negligible pressure $p_g \approx 0$:

$$J = K_r c_{s,sg}^2 \tag{24}$$

As for the gas phase systems, the fluxes are now non-dimensionalised (indicated also in this case by the apex *) by dividing their values by $DK_{s,s}\sqrt{p_l}/t$, where p_l is the partial pressure of the isotope Q in the liquid carrier, while the concentrations are non-dimensionalised by the factor $K_{s,l}\sqrt{p_l}$:

$$J^* = \frac{1}{\zeta}\left(1 - \frac{1}{K}c^*_{s,ls}\right) \tag{25}$$

$$J^* = \frac{1}{K}\left(c^*_{s,ls} - c^*_{s,sg}\right) \tag{26}$$

$$J^* = \frac{W}{K^2}c^{*2}_{s,sg} \tag{27}$$

We call *partition parameter* the dimensionless number ζ, introduced by Humrickhouse *et. al.* [25] and expressed here for a plane 1D geometry, is:

$$\zeta = \frac{D}{K_t}\frac{K_{s,s}}{K_{s,l}}\frac{1}{t} \tag{28}$$

Under steady state conditions, the three fluxes must be equal. Equating 25 and 26, it is possible to derive an expression for $c^*_{s,ls}$ as a function of $c^*_{s,sg}$:

$$c^*_{s,ls} = \frac{1}{\zeta + 1}\left(K + \zeta c^*_{s,sg}\right) \tag{29}$$

By substituting this value into the flux of Eq. 26, we get:

$$J^* = \frac{1}{\zeta+1}\left(1 - \frac{1}{K}c^*_{s,sg}\right) \quad (30)$$

The latter flux is equated with the surface flux expressed by Eq. 27, determining the concentration of tritium on the right side of the permeable membrane:

$$c^*_{s,sg} = \frac{\pm\sqrt{1+4W\left(\zeta+1\right)}-1}{2\frac{W}{K}\left(\zeta+1\right)} \quad (31)$$

The negative solution is unphysical because the denominator is strictly positive, so it is not considered. Finally, the solution for the steady-state flux through the system is given by Eq. 27:

$$J^* = \frac{\left(\sqrt{1+4W\left(\zeta+1\right)}-1\right)^2}{4W\left(\zeta+1\right)^2} \quad (32)$$

As evident, the flux is completely determined by the two dimensionless quantities ζ and W.

Even though the latter relation provides the solution for any value of the two dimensionless parameters, it is interesting to examine different limiting cases to verify the results. For $\zeta \ll 1$, the membrane effects are slower with respect to the mass transport in the liquid. This can be called membrane-limited regime (MLR). Taking the limit at $\zeta \to 0$ of Eq. 32, the following expression for the dimensionless flux is obtained:

$$J^* = \frac{\left(\sqrt{1+4W}-1\right)^2}{4W} \quad (33)$$

There are two limiting cases: when $W \ll 1$, surface effects dominate the kinetics, and the transport regime is surface-limited (SLR). In this case, the Taylor expansion of Eq. 32, evaluated near $W = 0$, gives the flux in the surface-limited regime:

$$J^* = W \quad (34)$$

which in dimensional form is $J = K_d p_l$. It is interesting to point out that this value is twice as high as the flux obtained in gas-phase systems in the surface-limited approximation, Eq. 9. Moreover, it is evident that W represents the dimensionless flux in the surface-limited regime. In the other case, $W \gg 1$, diffusion is the slowest phenomenon, so the regime is diffusion-limited (DLR). The flux becomes:

$$J^* = 1 \quad (35)$$

This means that the dimensional flux is $J = DK_{s,s}\sqrt{p_l}/t$, i.e. the flux obtained for gas-solid-gas systems in the diffusion-limited regime. In both cases analysed, the flux is independent of the mass transfer properties. Moreover, in the membrane-limited regime, the concentration on the left side of the membrane is $c^*_{s,ls} = K$, i.e. the dimensional concentration is $c_{s,ls} = K_{s,s}\sqrt{p_l}$ and thus depends only on the partial pressure of the tritium in the bulk of the fluid and on the solubility of the membrane. It is possible to calculate the concentration on the right side of the membrane directly from Equation 31, which simplifies under the membrane-limited regime to:

$$c^*_{s,sg} = \frac{\sqrt{1+4W}-1}{2\frac{W}{K}} \quad (36)$$

The dimensionless concentration on the low-pressure side is a function of a single variable, the permeation parameter W, and takes values ranging from 0 when the regime is diffusion-limited to 1 when the surface effects are rate-limiting. The concentration gradient between the liquid and the solid membrane is negligible in the case of surface-limited flux.

There are two possible cases for $\zeta \gg 1$. $\zeta \gg 1$ and $W > 1$ represents the condition where mass transport in the liquid is the rate-limiting phenomenon. The series expansion of the flux expressed by Equation 32 at $\zeta \to \infty$ is $1/\zeta + O\left(1/\zeta^2\right)$, so the flux in the liquid-limited regime (LLR) is:

$$J^* = \frac{1}{\zeta} \quad (37)$$

Thus, the partition parameter ζ represents the inverse of the dimensionless flux in the liquid-limited regime. Multiplied by the diffusion-limited flux, the dimensional flux for the liquid-limited regime became $J = K_t c_{l,b}$: the flux is independent of the membrane properties. For $\zeta \gg 1$ and $W < 1$, the regime lies between the liquid-limited and the surface-limited regimes and the flux is described by Equation 32.

Limiting cases can also be derived by taking the limits for W of Eq. 32 in a first step. If $W \ll 1$ and ζ is not particularly high, the limit for $W \to 0$ of the full flux is simply expressed by 34. If instead $\zeta \to \infty$, a mixed regime takes place, represented by Equation 32.

For $W >> 1$, taking the limit $W \to$ inf of Eq. 32:

$$J^* = \frac{1}{\zeta+1} \quad (38)$$

In dimensional form, the flux becomes $J = K_t c_{l,b}\zeta/\left(\zeta+1\right)$, which is the result of [25]. For $\zeta \gg 1$, the flux simply reduces to the LLR flux, Equation 37, and for $\zeta \ll 1$ to the DLR flux, Equation 35.

In Fig. 6, the relative error of the limit solutions with respect to the full solution, Eq. 32, is plotted as a function of W and ζ. The three dotted lines representing the $W = 1$, $\zeta = 1$ and $W = 1/\zeta$ planes divide the figure into three regions, namely the liquid-limited regime bounded by the $\zeta = 1$ and $W = 1/\zeta$ planes, the diffusion-limited regime lying between the $W = 1$ and $\zeta = 1$ planes, and the surface-limited regime in the remaining region. As in the gas-solid-gas system analysis, the graphs are truncated at $err = 0.05$. At $\zeta \ll 1$ and between the surface and the diffusion-limited regions, two intermediate regimes are defined, divided by the $W = 1$ plane. For

$4 \cdot 10^{-2} < W < 1$, the surface-dominating regime (SDR) occurs, while the diffusion-dominating regime (DDR) occurs for $1 < W < 4{\cdot}10^{2}$. The SDR can also be extended for larger values of ζ, in the neighbourhood of the SLR region bounded by the $W = 1/\zeta$ plane. The same considerations can be made for $W \gg 1$, where for $4 \cdot 10^{-}2 < \zeta < 1$ the regime is diffusion dominating, and for $1 < \zeta < 2 \cdot 10^{1}$ the liquid-dominating regime takes place. The latter is also found for smaller values of W, close to the LLR region and bounded by the plane $W = 1/\zeta$.

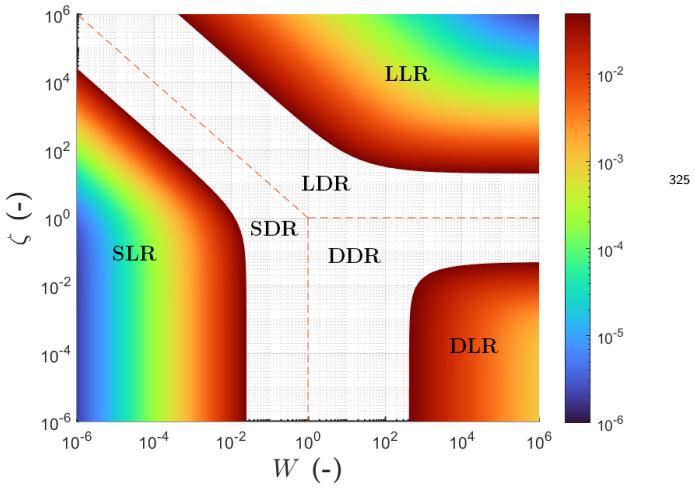

Figure 6: Relative error (-) between the limit regimes solution and the full solution Eq. 32, cut at $err = 0.05$.

The crucial point to emphasise here is that even at very high ζ the regime can still be limited by surface effects. This was not considered in the analysis of [25] and is of fundamental importance when the surface of the permeator is, for example, oxidized. Furthermore, if one considers the PAV extractor systems where the concentration of hydrogen isotopes in the liquid carrier decreases from the inlet to the outlet of the system, it is expected, when the permeation parameter at the inlet is not particularly high, that the permeation regime near the outlet of the permeator is surface-limited, since W depends on the bulk hydrogen partial pressure. The last point is that, for $\zeta < 1$, a "pure" diffusion limited regime occurs only for $W > 4{\cdot}10^{2}$. For smaller value, surface effects play still a non-negligible role.

Table 1 shows the summary of the introduced dimensionless quantities and their meaning in the limiting cases, with the corresponding expression for the dimensionless flux J^*. MR stands for mixed regime.

It is interesting to highlight that the three non-dimensional quantities introduced in this section, i.e. the permeation parameter W, the partition parameter ζ and the contact parameter C, are directly related. Recalling that the permeation parameter represent the ratio between surface and diffusion properties, the partition parameter the ratio between diffusion and mass transport in the liquid and, lastly,

Regime J^*	$W \ll 1$	$W < 1$	$W > 1$	$W \gg 1$
$\zeta \gg 1$	MR Eq. 32	LLR $J^* = 1/\zeta$	LLR $J^* = 1/\zeta$	LLR $J^* = 1/\zeta$
$\zeta > 1$	SLR $J^* = W$	MR Eq. 32	MR Eq. 32	LDR $J^* = 1/(\zeta + 1)$
$\zeta < 1$	SLR $J^* = W$	MR Eq. 32	MR Eq. 32	DDR $J^* = 1/(\zeta + 1)$
$\zeta \ll 1$	SLR $J^* = W$	SDR Eq. 33	DDR Eq. 33	DLR $J^* = 1$

Table 1: Summary of the transport regimes depending on the dimensionless quantities introduced.

the contact parameter the ratio between transport in the liquid and surface effects, the product between two of them gives the inverse of the remaining multiplied by ratio of the dissociation constants of the solid and liquid, thus:

$$W\zeta C = \frac{K_{d,s}}{K_{d,l}} = K^2 \frac{K_{r,s}}{K_{r,l}} \tag{39}$$

3. Axial Hydrogen isotope transport in permeators

3.1. Liquid-gas systems

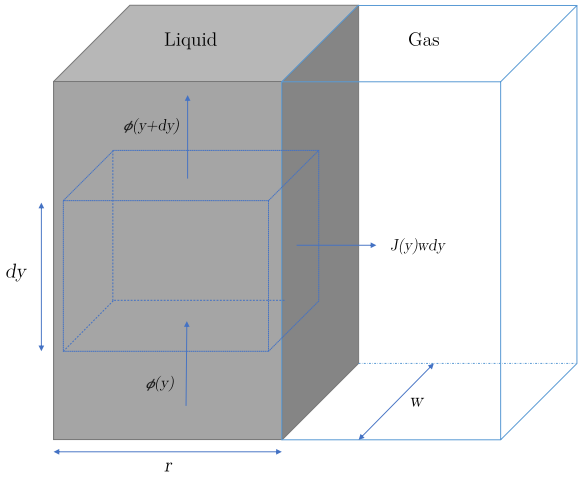

Figure 7: Hydrogen isotope balance on a liquid volume in liquid-gas systems.

The axial transport in a rectangular channel of liquid carrier of thickness r and width w is analysed. Considering a small volume $rwdy$, shown in Fig. 7, the molar balance can be expressed by:

$$\phi\,(y) = \phi\,(y + dy) + J\,(y)\,wdy \tag{40}$$

The molar rate is given by $\phi\,(y) = vrwc_{l,b}\,(y)$, where v (m s^{-1}) is the fluid velocity. Differentiating, the molar balance becomes:

$$\frac{dc_{l,b}\,(y)}{dy} = -\frac{1}{vr} J\,(y) \tag{41}$$

The equation can be non-dimensionalized dividing the geometrical parameters by the total channel length H, the concentrations by the inlet concentration $c_{l,b}(0) = K_{s,l}\sqrt{p_{l,0}}$ and the flux by the liquid-limited flux $K_t c_{l,b}$. It gives:

$$\frac{dc^*_{l,b}(y^*)}{dy^*} = -\tau J^*(y^*)\, c^*_{l,b}(y^*) \tag{42}$$

Where $\tau = HK_t/v/r$ (-) and the non-dimensional flux

$$J^*(y^*) = \frac{\left(\sqrt{1+4/C(y^*)}-1\right)^2}{4/C(y^*)} \tag{43}$$

with $C(y^*) = C(0)/c^*_{l,b}(y^*)$. Equation 42 can be solved analytically in the two limit cases liquid-limited regime and surface-limited regime. If $C(0) \ll 1$, the dimensionless radial flux becomes equal to 1, therefore Eq. 42 simply becomes:

$$\frac{dc^*_{l,b}(y^*)}{dy^*} = -\tau c^*_{l,b}(y^*) \tag{44}$$

which has the solution, with $c^*_{l,b}(0) = 1$:

$$c^*_{l,b}(y^*) = e^{-\tau y^*} \tag{45}$$

The dimensional concentration is:

$$c_{l,b}(y) = c_{l,b}(0)\, e^{-\tau \frac{y}{H}} \tag{46}$$

If instead $C(0) >> 1$, the kinetics is limited by surface effects. Injecting the expression of J^* given by Eq. 20, the molar balance becomes:

$$\frac{dc^*_{l,b}(y^*)}{dy^*} = -\frac{\tau}{C(y^*)} c^*_{l,b}(y^*) = -\frac{\tau}{C(0)} c^{*2}_{l,b}(y^*) \tag{47}$$

The solution, for $c^*_{l,b}(0) = 1$, is:

$$c^*_{l,b}(y^*) = \frac{1}{\frac{\tau}{C(0)} y^* + 1} \tag{48}$$

In dimensional form becomes:

$$c_{l,b}(y) = \frac{c_{l,b}(0)}{\frac{\tau}{C(0)}\frac{y}{H} + 1} \tag{49}$$

The efficiency of the permeator can be expressed by the ratio between the drop in the concentration between the inlet and the outlet over the inlet concentration, mathematically:

$$\eta = \frac{c_{l,b}(0) - c_{l,b}(H)}{c_{l,b}(0)} = 1 - \frac{c_{l,b}(H)}{c_{l,b}(0)} = 1 - \frac{c^*_{l,b}(1)}{c^*_{l,b}(0)} \tag{50}$$

In liquid-limited regime, the efficiency becomes:

$$\eta = 1 - e^{-\tau} \tag{51}$$

This means that in the LLR the efficiency is only determined by τ, and it can be increased increasing the length of the permeator, decreasing fluid velocity and/or channel thickness. The efficiency for the surface-limited regime is:

$$\eta = 1 - \frac{1}{\frac{\tau}{C(0)} + 1} \tag{52}$$

The SLR efficiency increases, as in the LLR regime, increasing τ. In order to have η different from zero, τ much bigger than 1 is required, and it must be bigger than $C(0)$ if high efficiencies are needed ($\tau = C(0)$ gives $\eta = 0.5$).

If an intermediate regime takes place ($C(0)$ around 1), the concentration distribution along y can be obtained with a simple finite differences numerical scheme that solves Eq. 42, and the efficiency injecting the obtained $c^*_{l,b}(1)$ in Equation 50.

It must be addressed the fact that, being $C(y^*)$ inversely proportional to the concentration $c^*_{l,b}(y^*)$ that decreases moving on the axial coordinate, the contact parameter is a monotonically increasing function of y^*. Therefore, if the efficiency of the system is particularly high and/or $C(0)$ is not sufficiently smaller than 1, the contact parameter may reach values around 1 along the channel and the regime departs from the liquid-limited regime. In this case the relation given by Equation 51 overestimates the efficiency. In order to be sure that the LLR efficiency relation holds, it must be checked that the contact parameter at the exit of the permeator, $C(1)$, is still $\ll 1$, or equivalently $C(1) = C(0)\, e^{\tau} \ll 1$. If this is not true, the solution of the problem has to be found numerically with Eq. 42.

3.2. Liquid-solid-gas systems

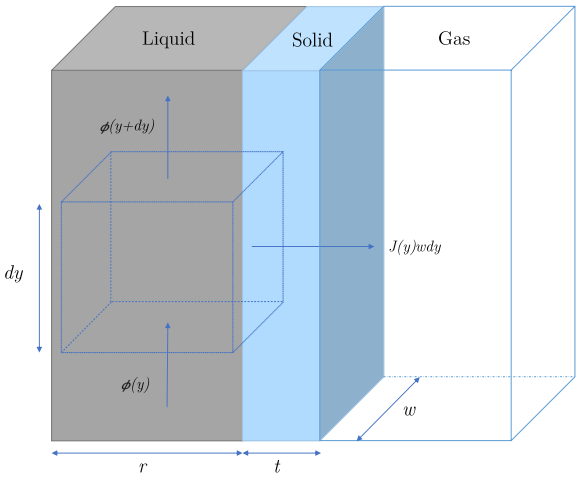

Figure 8: Hydrogen isotope balance on a liquid volume in liquid-solid-gas systems.

The axial transport in a rectangular channel of liquid carrier of thickness r and width w, separated from a

side kept under vacuum by a metallic membrane of thickness t, is analysed. Following the same strategy adopted in the latter section, the differential equation expressing the concentration distribution is given by equation 41. It can be non-dimensionalized dividing the concentrations by $K_{s,l}\sqrt{p_l\left(0\right)}$ and the flux by $DK_{s,s}\sqrt{p_l\left(0\right)}/t$. It gives:

$$\frac{dc_{l,b}^{*}\left(y^{*}\right)}{dy^{*}}=-\tau\zeta J^{*}\left(y^{*}\right)c_{l,b}^{*}\left(y^{*}\right) \tag{53}$$

where the dimensionless radial flux is:

$$J^{*}\left(y^{*}\right)=\frac{\left(\sqrt{1+4W\left(y^{*}\right)\left(\zeta+1\right)}-1\right)^{2}}{4W\left(y^{*}\right)\left(\zeta+1\right)^{2}} \tag{54}$$

Here $W\left(y^{*}\right)=W\left(0\right)c_{l,b}^{*}\left(y^{*}\right)$. The differential equation can be solved analytically for the three limit regimes. When $W\gg1$ and $\zeta\gg1$ the liquid-limited regime takes place, and adopting the corresponding radial flux, it is:

$$\frac{dc_{l,b}^{*}\left(y^{*}\right)}{dy^{*}}=-\tau c_{l,b}^{*}\left(y^{*}\right) \tag{55}$$

This equation can be easily integrated, giving, for $c_{l,b}^{*}\left(0\right)=1$:

$$c_{l,b}^{*}\left(y^{*}\right)=e^{-\tau y^{*}} \tag{56}$$

And in dimensional form:

$$c_{l,b}\left(y\right)=c_{l,b}\left(0\right)e^{-\tau\frac{y}{H}} \tag{57}$$

It is interesting to see that the solution is equivalent to the liquid-gas case, the membrane has no effect on the radial flux and therefore on the axial concentration distribution. The efficiency of the PAV is therefore equivalent to Eq. 51:

$$\eta=1-e^{-\tau} \tag{58}$$

If instead, $\zeta\ll1$ and $W\gg1$, the regime is diffusion-limited. Eq. 53 becomes:

$$\frac{dc_{l,b}^{*}\left(y^{*}\right)}{dy^{*}}=-\tau\zeta c_{l,b}^{*}\left(y^{*}\right) \tag{59}$$

It has the solution:

$$c_{l,b}^{*}\left(y^{*}\right)=e^{-\tau\zeta y^{*}} \tag{60}$$

In dimensional form:

$$c_{l,b}\left(y\right)=c_{l,b}\left(0\right)e^{-\tau\zeta\frac{y}{H}} \tag{61}$$

The efficiency in the DLR case becomes:

$$\eta=1-e^{-\tau\zeta} \tag{62}$$

The efficiency in this case does not depend on the transport in the liquid. This can be seen expanding the product between τ and ζ, in which the mass transfer coefficient K_t disappears.

The last limit regime happens when $\zeta\ll1$ and $W\ll1$. In the surface-limited regime the differential equation for the bulk concentration is:

$$\frac{dc_{l,b}^{*}\left(y^{*}\right)}{dy^{*}}=-\tau\zeta W\left(0\right)c_{l,b}^{*2}\left(y^{*}\right) \tag{63}$$

That gives the following axial concentration distribution:

$$c_{l,b}^{*}\left(y^{*}\right)=\frac{1}{\tau\zeta W\left(0\right)y^{*}+1} \tag{64}$$

The dimensional surface-limited axial concentration is therefore given by:

$$c_{l,b}\left(y\right)=\frac{c_{l,b}\left(0\right)}{\tau\zeta W\left(0\right)\frac{y}{H}+1} \tag{65}$$

The efficiency in the SLR becomes:

$$\eta=1-\frac{1}{\tau\zeta W\left(0\right)+1} \tag{66}$$

It is interesting to highlight that the solution is equivalent to the one for the liquid-gas system, exchanging the surface properties of the liquid with the one of the solid membrane. Injecting Equation 39 to the axial concentration gives:

$$c_{l,b}^{*}\left(y^{*}\right)=\frac{1}{\frac{\tau}{C(0)}\frac{K_{d,s}}{K_{d,l}}y^{*}+1} \tag{67}$$

4. Conclusions and future work

This paper presents new mathematical models for tritium transport in liquid-phase, both for liquid-gas and liquid-solid-gas systems. For the first kind, the contact parameter C is defined, and it is used to define the transport regime and to express the relation for the general flux. For liquid-solid-gas systems, the model uses two dimensionless parameters, W and ζ, and allows to define different regions where the transport kinetics can be limited by surface effects, diffusion and mass transfer, or a mixed regime in between. In addition, a general relation that gives the value of the permeation flux in the mixed regime is derived, and the simplified equations in the limit regimes are presented. In a second part, the axial transport for a simple geometry is derived, both for the Liquid-Vacuum Contactor and the Permeator Against Vacuum, giving simple relations for the efficiency of the systems derived in the limit regimes.

It should be highlighted that the expressions derived for the tritium permeation flux in the different regimes and in the different systems can be used in the particular case where the concentration in the liquid or the pressure in the gas are known quantities; in more complex applications, this does not happen. For example, in the Water-Cooled Lithium-Lead (WCLL) breeding blanket of the European DEMO reactor [26] or in WCLL Test Blanket Module of ITER [27], the concentration in the liquid is derived from mass balance equations [28, 29, 30, 31, 32, 23], which depend on the permeation in the various domains

and which, in turn, depend on the concentration. Therefore, implicit equations have to be solved and numerical schemes must be adopted. With the expressions of the tritium fluxes derived in this paper, it becomes easier to set tritium transport analytical models not only in DLR but also in SLR.

Future work will regard two main aspects. Firstly, the models developed will be applied to the design of HPS, LVC and PAV systems under fusion-relevant operative conditions. Secondly, experiments on the hydrogen/deuterium permeation in a liquid-solid-gas system are on-going in a dedicated apparatus, located at ENEA Brasimone research center, called HyPer-QuarCh II. In particular, concerning this last point, a detailed overview of the experimental set-up of this laboratory-scale device can be found in [33]. The facility can be used to characterize HPS and, hence, it will be possible to validate the model developed over the experimental results obtained.

References

[1] A. Ciampichetti, M. Zucchetti, I. Ricapito, M. Utili, A. Aiello, G. Benamati, Performance of a hydrogen sensor in Pb–16Li, Journal of Nuclear Materials 367-370 (2007) 1090–1095, proceedings of the Twelfth International Conference on Fusion Reactor Materials (ICFRM-12). doi:https://doi.org/10.1016/j.jnucmat.2007.03.250.

[2] I. Nicolotti, M. Utili, L. Candido, M. Zucchetti, A hydrogen sensor for liquid-metal breeding blankets, Transactions of the American Nuclear Society 112 (2015) 193–196, 2015 ANS Annual Meeting, San Antonio, TX.

[3] L. Candido, I. Nicolotti, M. Utili, M. Zucchetti, Design optimization of a hydrogen sensor for ITER Pb16Li blankets, IEEE Transactions on Plasma Science 45 (7) (2017) 1831–1836. doi:10.1109/TPS.2017.2710218.

[4] L. Candido, M. Cantore, E. Galli, R. Testoni, M. Zucchetti, M. Utili, A. Ciampichetti, Characterization of Pb-15.7Li hydrogen isotopes permeation sensors and upgrade of HyPer-Quarch experimental device, IEEE Transactions on Plasma Science 48 (6) (2020) 1505–1511. doi:10.1109/TPS.2020.2974937.

[5] I. Ricapito, A. Ciampichetti, R. Lässer, Y. Poitevin, M. Utili, Tritium extraction from liquid Pb-16Li: A critical review of candidate technologies for ITER and DEMO applications, Fusion Science and Technology 60 (3) (2011) 1159–1162. doi:https://doi.org/10.13182/FST11-A12621.

[6] D. Demange, R. Antunes, O. Borisevich, L. Frances, D. Rapisarda, A. Santucci, M. Utili, Tritium extraction technologies and demo requirements, Fusion Engineering and Design 109-111 (2016) 912–916. doi:https://doi.org/10.1016/j.fusengdes.2016.01.053.

[7] B. Garcinuño, D. Rapisarda, I. Fernández-Berceruelo, D. Jiménez-Rey, J. Sanz, C. Moreno, I. Palermo, Ángel Ibarra, Design and fabrication of a permeator against vacuum prototype for small scale testing at lead-lithium facility, Fusion Engineering and Design 124 (2017) 871–875. doi:https://doi.org/10.1016/j.fusengdes.2017.02.060.

[8] F. Okino, P. Calderoni, R. Kasada, S. Konishi, Feasibility analysis of vacuum sieve tray for tritium extraction in the hcll test blanket system, Fusion Engineering and Design 109-111 (2016) 1748–1753. doi:https://doi.org/10.1016/j.fusengdes.2015.10.004.

[9] F. Papa, et al., Engineering design of a permeator against vacuum mock-up with niobium membrane, Fusion Engineering and Design 166.

[10] G. Federici, L. Boccaccini, F. Cismondi, M. Gasparotto, Y. Poitevin, I. Ricapito, An overview of the eu breeding blanket design strategy as an integral part of the demo design effort, Fusion Engineering and Design 141 (2019) 30–42. doi:doi.org/10.1016/j.fusengdes.2019.01.141.

[11] A. Pisarev, V. Shestakov, R. Hayakawa, Y. Hatano, K. Watanabe, Gas-driven hydrogen permeation in the surface-limited regime, Journal of Nuclear Materials 320 (3) (2003) 214–222. doi:https://doi.org/10.1016/S0022-3115(03)00110-7.

[12] M. Baskes, A calculation of the surface recombination rate constant for hydrogen isotopes on metals, Journal of Nuclear Materials 92 (2) (1980) 318–324. doi:https://doi.org/10.1016/0022-3115(80)90117-8.

[13] K. Pick, M. A.; Sonnenberg, A model for atomic hydrogen-metal interactions — application to recycling, recombination and permeation, Journal of Nuclear Materials 131 (1985) 208–220.

[14] I. Ali-Khan, K.J. Dietz, F.G. Waelbroeck, P.Wienhold, The rate of hydrogen release out of clean metallic surfaces, Journal of Nuclear Materials 76-77 (1978) 337–343.

[15] Hydrogen isotope permeation through and inventory in the first wall of the water cooled pb–17li blanket for demo, Journal of Nuclear Materials 273 (1) (1999) 66–78. doi:https://doi.org/10.1016/S0022-3115(99)00015-X.

[16] O. V. Ogorodnikova, X. Raepsaet, M. A. Fütterer, Tritium permeation through the first wall of the eu-hcpb blanket, Fusion Engineering and Design 49-50 (2000) 921–926. doi:https://doi.org/10.1016/S0920-3796(00)00339-2.

[17] O. Ogorodnikova, Surface effects on plasma-driven tritium permeation through metals, Journal of Nuclear Materials 290-293 (2001) 459–463. doi:https://doi.org/10.1016/S0022-3115(00)00642-5.

[18] E. Hodille, X. Bonnin, R. Bisson, T. Angot, C. Becquart, J. Layet, C. Grisolia, Macroscopic rate equation modeling of trapping/detrapping of hydrogen isotopes in tungsten materials, Journal of Nuclear Materials 467 (2015) 424–431. doi:https://doi.org/10.1016/j.jnucmat.2015.06.041.

[19] R. Delaporte-Mathurin, E. Hodille, J. Mougenot, G. D. Temmerman, Y. Charles, C. Grisolia, Parametric study of hydrogenic inventory in the iter divertor based on machine learning, Scientifc Reports 10 (2020) 17798. doi:https://doi.org/10.1038/s41598-020-74844-w.

[20] R. Arredondo, K. Schmid, F. Subba, G. Spagnuolo, Preliminary estimates of tritium permeation and retention in the first wall of demo due to ion bombardment, Nuclear Materials and Energy 28 (2021) 101039. doi:https://doi.org/10.1016/j.nme.2021.101039.

[21] R. Delaporte-Mathurin, H. Yang, J. Denis, J. Dark, E. A. Hodille, G. D. Temmerman, X. Bonnin, J. Mougenot, Y. Charles, H. Bufferand, G. Ciraolo, C. Grisolia, Fuel retention in WEST and ITER divertors based on FESTIM monoblock simulations, Nuclear Fusion 61 (12) (2021) 126001. doi:10.1088/1741-4326/ac2bbd.

[22] L. Candido, C. Alberghi, Verification and validation of mHIT code over TMAP for hydrogen isotopes transport studies in fusion-relevant environments, Fusion Engineering and Design 172.

[23] J. Dark, R. Delaporte-Mathurin, Y. Charles, E. A. Hodille, C. Grisolia, J. Mougenot, Influence of hydrogen trapping on WCLL breeding blanket performances, Nuclear Fusion 61 (11) (2021) 116076. doi:10.1088/1741-4326/ac28b0.

[24] F. Montupet-Leblond, L. Corso, M. Payet, R. Delaporte-Mathurin, E. Bernard, Y. Charles, J. Mougenot, S. Vartanian, E. Hodille, C. Grisolia, Permeation and trapping of hydrogen in eurofer97, Nuclear Materials and Energy 29 (2021) 101062. doi:https://doi.org/10.1016/j.nme.2021.101062.

[25] P. W. Humrickhouse, B. J. Merrill, Vacuum permeator analysis for extraction of tritium from dcll blankets, Fusion Science and Technology 68 (2015) 295–302.

[26] A. Del Nevo, P. Arena, G. Caruso, P. Chiovaro, P. Di Maio, M. Eboli, F. Edemetti, N. Forgione, R. Forte, A. Froio, F. Giannetti, G. Di Gironimo, K. Jiang, S. Liu, F. Moro, R. Mozzillo, L. Savoldi, A. Tarallo, M. Tarantino, A. Tassone, M. Utili,

R. Villari, R. Zanino, E. Martelli, Recent progress in developing a feasible and integrated conceptual design of the wcll bb in eurofusion project, Fusion Engineering and Design 146 (2019) 1805–1809. doi:https://doi.org/10.1016/j.fusengdes.2019.03.040.

[27] J. Aubert, G. Aiello, D. Alonso, T. Batal, R. Boullon, S. Burles, B. Cantone, F. Cismondi, A. Del Nevo, L. Maqueda, A. Morin, E. Rodríguez, F. Rueda, M. Soldaini, J. Vallory, Design and preliminary analyses of the new water cooled lithium lead tbm for iter, Fusion Engineering and Design 160 (2020) 111921. doi:https://doi.org/10.1016/j.fusengdes.2020.111921.

[28] F. Franza, A. Ciampichetti, I. Ricapito, M. Zucchetti, A model for tritium transport in fusion reactor components: The FUS-TPC code, Fusion Engineering and Design 87 (4) (2012) 299–302. doi:https://doi.org/10.1016/j.fusengdes.2012.01.002.

[29] L. Candido, M. Utili, I. Nicolotti, M. Zucchetti, Tritium transport in HCLL and WCLL DEMO blankets, Fusion Engineering and Design 109-111 (2016) 248–254. doi:https://doi.org/10.1016/j.fusengdes.2016.03.017.

[30] A. Santucci, S. Tosti, F. Franza, Model improvements for tritium transport in DEMO fuel cycle, Fusion Engineering and Design 98-99 (2015) 1880–1884. doi:https://doi.org/10.1016/j.fusengdes.2015.05.050.

[31] C. Alberghi, L. Candido, R. Testoni, M. Utili, M. Zucchetti, Magneto-convective effect on tritium transport at breeder unit level for the wcll breeding blanket of demo, Fusion Engineering and Design 160 (2020) 111996. doi:https://doi.org/10.1016/j.fusengdes.2020.111996.

[32] L. Candido, C. Alberghi, F. Moro, S. Noce, R. Testoni, M. Utili, M. Zucchetti, A novel approach to the study of magnetohydrodynamic effect on tritium transport in WCLL breeding blanket of demo, Fusion Engineering and Design 167 (2021) 112334. doi:https://doi.org/10.1016/j.fusengdes.2021.112334.

[33] L. Candido, C. Alberghi, A. Antonelli, S. Bassini, M. Piccioni, S. Storai, R. Testoni, M. Utili, M. Zucchetti, HyPer-QuarCh II: a laboratory-scale device for hydrogen isotopes permeation experiments, Fusion Engineering and Design 172 (2021) 112920. doi:https://doi.org/10.1016/j.fusengdes.2021.112920.